

Wavelength-Domain Simulation of Multiwavelength Optical Networks

Ioannis Roudas, Neophytos Antoniadis, *Member, IEEE*, Dwight H. Richards, *Member, IEEE*, Richard E. Wagner, Janet Lehr Jackel, *Senior Member, IEEE*, Sarry F. Habiby, Thomas E. Stern, *Member, IEEE*, and Aly F. Elrefaie

Invited Paper

Abstract—This paper presents an efficient simulation method for the design of the optical transport layer of large-scale multiwavelength optical networks. According to this method, computations are performed in two complementary steps. During the first step, the powers of optical signals, amplified spontaneous emission (ASE) noise, and linear optical crosstalk are calculated at all points in the network. During the second step, the distortion and the overall performance of selected optical paths in the network are calculated. Each simulation step requires a different computer representation of optical signals and network components. A large part of this paper is devoted to the description of the wavelength-domain representation used during the first simulation step. In wavelength domain, optical signals are represented by their carrier wavelength and average power, exclusively. In addition, the network components are fully characterized by their loss or gain as a function of wavelength. The phase-transfer functions of the network components are discarded. These simplifications result in a dramatic increase in execution speed. During the second simulation step, optical signals are represented by their temporal waveforms. Linear optical network segments are replaced by an equivalent channel. The link between the two simulation steps is explained in detail. The remainder of the paper is devoted to the implementation of a network simulation tool based on the above method in the context of the multiwavelength optical networking (MONET) project. To illustrate the capabilities of the MONET simulator, a mesh of 4×4 wavelength-selective cross-connects (WSXC's) and wavelength add-drop multiplexers (WADM's) is studied and the crosstalk performance is determined.

Index Terms—Optical crosstalk, optical switches, simulation, wavelength-division multiplexing.

Manuscript received September 22, 1999; revised December 22, 1999. This work was supported by the MONET consortium under DARPA funding agreement MDA 972-95-3-0027.

I. Roudas was with Telcordia Technologies (formerly Bell Communications Research). He is now with Corning Inc., Somerset, NJ 08873 USA.

N. Antoniadis was with the Center for Telecommunications Research, Department of Electrical Engineering, Columbia University, Schapiro Research Building, New York, NY 10027 USA. He is now with Corning Inc., Somerset, NJ 08873 USA.

D. H. Richards and J. L. Jackel are with Telcordia Technologies (formerly Bell Communications Research), Red Bank, NJ 07701 USA.

R. E. Wanger was with Telcordia Technologies (formerly Bell Communications Research). He is now with Corning Inc., Corning, NY 14831 USA.

S. F. Habiby was with Telcordia Technologies (formerly Bell Communications Research). He is now with Tellium Inc., Oceanport, NJ 07757 USA.

T. E. Stern is with the Center for Telecommunications Research, Department of Electrical Engineering, Columbia University, Schapiro Research Building, New York, NY 10027 USA.

A. F. Elrefaie was with Telcordia Technologies (formerly Bell Communications Research). He is now with Lucent Technologies, Wireless Broadband Networks Division, Milpitas, CA 95035 USA.

Publisher Item Identifier S 1077-260X(00)03446-8.

I. INTRODUCTION

AS MULTIWAVELENGTH optical networking approaches commercialization, the development of software tools for network performance evaluation and design emerges as an important issue.

Computer modeling of the physical (i.e., optical transport) layer of multiwavelength optical networks is a challenging task, due to the large number of network components and reconfigurable links. In addition, for the evaluation of the end-to-end network performance, it is necessary to take into account the impact of several transmission impairments, e.g., amplified spontaneous emission (ASE) noise accumulation, crosstalk, polarization-dependent loss, polarization-mode dispersion (PMD), chromatic dispersion, nonlinearities, chirp, signal distortion due to filtering, reflections, and so forth. Because of the complexity of the problem, the choice of an adequate computer representation of optical signals and network components is essential.

Several software products for the study of point-to-point optical communication systems and optical networks are currently commercially available (e.g., PTDS [1], HP EEs of [2], OptSim [3], FOCUSS [4], [5], COMSIS [6], LinkSIM [7]). Despite their differences in implementation, the number of built-in modules and the level of detail in the models of individual components, these simulators are mainly based on the same well-established strategy, namely, waveform-level simulation [8], [9].¹ As explained in the following section, the computation time required for large multiwavelength optical networks makes this straightforward approach in many cases impractical, if not impossible, with current computer capabilities. Therefore, a different, network-oriented simulation strategy is necessary.

One of the goals of the multiwavelength optical networking (MONET) project [11] is to create a simulation tool for efficient computation of the end-to-end performance of various multiwavelength optical network topologies and optimal design of network elements.

This paper presents in detail the simulation strategy used in the MONET simulation tool. In this tool, the computations are performed in two complementary steps. During the first step, the tool calculates the power of optical signal, ASE noise, and linear crosstalk at all points in the network. During the second

¹In these simulators, a wavelength-domain representation of the optical signals is used for the modeling of Erbium-doped fiber amplifiers [10]. Recently, PTDS and FOCUSS demonstrated wavelength-domain capabilities for other optical network components.

step, the tool calculates the distortion and the overall performance of selected optical paths in the network. Each simulation step requires a different computer representation of optical signals and network components. During the first simulation step, a wavelength-domain representation [10], [12] of the optical signals and network components is used. This representation stems from the spectrally resolved model of erbium-doped fiber amplifiers (EDFA's) [10]. Optical signals are represented by their carrier wavelength and average power exclusively, and not by their temporal waveform, as is customary in waveform-level simulation [8], [9]. In addition, the network components are fully characterized by their loss or gain as a function of wavelength. The phase-transfer functions of the network components are discarded. These simplifications result in a dramatic increase in execution speed. The drawback is that impairments that cause waveform distortion cannot be studied in the wavelength domain. Therefore, a second simulation step is required to associate the incomplete results provided by the wavelength-domain simulation with the system performance. During the second simulation step, optical signals are represented by their temporal waveforms. Linear optical network segments are replaced by an equivalent channel. The link between the two simulation steps is explained in detail.

A network simulation tool based on the above strategy is implemented in the context of the MONET project. To illustrate its capabilities, the MONET simulation tool is used to evaluate the performance of a mesh of 4×4 wavelength-selective cross-connects (WSXC's) and wavelength add-drop multiplexers (WADM's).

The remainder of the paper is organized as follows. Section II is an overview of the major operational principles of the MONET simulation tool. Section III presents the essential features of the simulation environment used for the implementation of the MONET simulation tool. Section IV describes the library of optical modules and the computer implementation of the wavelength-domain representation in the MONET simulation tool. In Section V, a mesh network topology is described and simulated. In Appendix A, the reasons for the wavelength-domain representation of optical linear crosstalk are explained in detail. Finally, in Appendix B, the multipath interference between ASE noise components is analyzed.

II. SIMULATION PRINCIPLES

A. Waveform-Level Simulation of Optical Signals

In order to understand the wavelength-domain representation, it is useful first to summarize briefly the principles of the waveform-level simulation.

The waveform-level simulation is based on the computer representation of signals by sets of samples either on the time or frequency domain.

In time domain, bandlimited continuous-time signals can be fully modeled by discrete-time signals sampled with a frequency higher than or equal to the Nyquist rate [13]. Digital signal processing techniques are used for the modeling of various optical components [14].

Since individual optical signals are narrowband, their equivalent low-pass representation is used to reduce the sampling fre-

quency [14]. However, even so, due to the broad aggregate bandwidth of wavelength-division multiplexed (WDM) signals (usually several orders of magnitude larger than the bit rate of an individual optical signal), a complete time-domain representation would result in huge oversampling. Therefore, waveform-level simulations based on a time-domain representation are computationally intensive for the study of complex multiwavelength optical networks and are limited mainly to point-to-point WDM systems or network subsystems.

A frequency-domain representation is more adequate in the case of linear systems because it allows convolutions to be done efficiently ([9, p. 560]). According to this technique, the time-domain signals from the information and noise sources are sampled and transformed to frequency domain using the discrete Fourier transform (DFT). The cascade of linear elements is replaced by a single transfer function. At the output of the last module, the output spectrum samples are transformed to time domain using the inverse DFT.

Time- and frequency-domain representations are equivalent. Current commercial software products for the study of point-to-point optical communication systems have both time- and frequency-domain capabilities. These capabilities might be used simultaneously, e.g., in the modeling of nonlinear propagation in optical fibers where a split-step Fourier method is used to solve the nonlinear Schrödinger equation [15].

B. Wavelength-Domain Representation of Optical Signals and ASE Noise

As mentioned in Section I, a different method is proposed here for the simulation of multiwavelength optical networks. Computations are performed in two steps.

During the first step, power computations are done using a simplified representation of optical signals and network components at the optical transport layer of multiwavelength optical networks. This representation stems from the spectrally resolved model of EDFA's [10]. It is assumed that the network components do not alter the shape of the signal waveforms, i.e., signal distortion due to linear or nonlinear effects is ignored. Based on the above assumption, the modulation of optical signals is ignored since it is not influenced by the WDM optical network element components. Furthermore, optical signals are represented by their carrier wavelength and average power exclusively.

For the computer representation of the optical signals, the wavelength axis is discretized into N wavelength bins. The choice of the wavelength bin size is arbitrary and depends on the desired accuracy [10]. Typically, the wavelength bin size is several times the bit rate. The central wavelengths of these wavelength bins define a grid.

The representation of the optical signals differs depending on whether they occupy one or several wavelength bins (defined as narrow-band or wide-band optical signals, respectively). We distinguish two different types of optical signals, namely, optical signals produced by laser sources (narrow-band) and ASE noise (wide-band). Each type is represented separately. 1) Optical signals produced by laser sources are represented by a pair of numbers (carrier wavelength, average power). 2) Forward and backward ASE noises are represented by N pairs of numbers

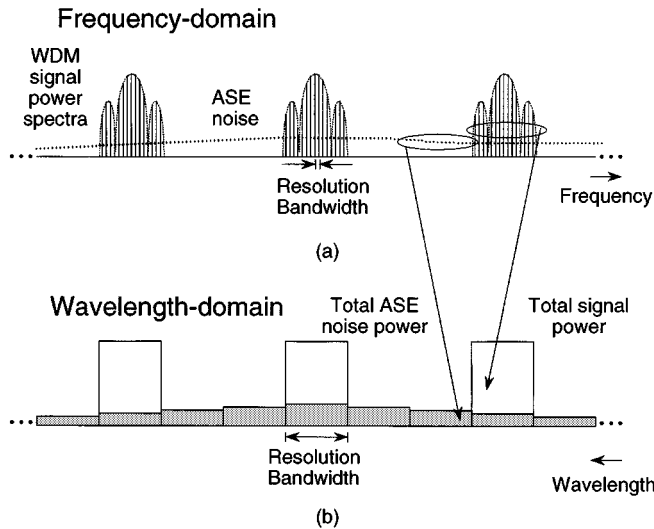


Fig. 1. Power spectra: (a) frequency-domain representation and (b) wavelength-domain representation. Symbols: white rectangles: total signal power; shaded rectangles: total ASE noise power. The resolution bandwidth in the wavelength-domain can be nonuniform.

[i.e., (wavelength node, average ASE power at this node of the wavelength grid)].

Fig. 1(a) and (b) compares the waveform-level frequency-domain representation with the proposed representation. In the frequency domain [Fig. 1(a)], a WDM signal is represented by sets of samples of the magnitude and phase spectra throughout the frequency band of interest [in Fig. 1(a), only the power spectrum is shown]. The resolution is equal to the reciprocal of the signal duration and consequently, is a small fraction of the bit rate. In the proposed representation, the spectral components are grouped in larger bins [Fig. 1(b)]. Since the resolution bandwidth is much coarser in the proposed representation than in the frequency domain, we call this representation a *wavelength-domain representation*.²

It is worth noting that the wavelength-domain representation of the optical signals is similar to that of an optical spectrum analyzer. However, there is a fundamental difference between the way a spectrum analyzer operates and wavelength-domain simulation: In reality, signals carry information that the spectrum analyzer cannot discern. In the wavelength-domain simulation case, information is not even transmitted.

It must be stressed that time-domain aliasing due to the coarse resolution in the wavelength domain does not pose an issue here since the wavelength-domain representation is not used to evaluate the evolution of signal waveforms, but only average signal powers. No passage from the wavelength-domain representation to the waveform-level time-domain representation is possible.

²The name “wavelength-domain representation” might be confusing at first. Obviously, the notions of frequency and wavelength are equivalent since there is a one-to-one correspondence between them. As shown in Fig. 1(a) and (b), one fundamental difference between the proposed representation and the more conventional frequency-domain representation is the resolution bandwidth. The name “wavelength-domain representation” is intended to be reminiscent of this difference, similar to the distinction between wavelength-division multiplexing and frequency-division multiplexing. Similar approaches in the bibliography exist under different names, e.g., [16].

Another important parameter of the wavelength-domain representation is the *simulation bandwidth*. The adequate choice of this parameter is discussed in more detail in [10].

The above representation can be extended to include linear optical crosstalk, as explained below.

C. Wavelength-Domain Representation of Linear Optical Crosstalk

Optical crosstalk is a major impairment in WDM optical communications systems and networks. It can lead to error floors and imposes severe requirements on the components, e.g., [17]–[31].

Depending on the nature of the physical effects involved in its generation, optical crosstalk can be classified as *linear* or *nonlinear* [32]. Linear crosstalk is due to nonideal optical multiplexer/demultiplexers (MUX/DMUX’s) and optical space switches contained in WADM’s and optical cross-connects [20], [21]. Nonlinear crosstalk is due to nonlinearities in optical fibers and other components, e.g., wavelength converters [22], [23]. In wavelength-domain representation, we limit our interest to linear crosstalk exclusively.

Optical crosstalk can also be distinguished [33] as *common-channel* (also referred to as homowavelength, intrachannel, or intraband) and *adjacent-channel* (also referred to as heterowavelength, interchannel, or interband). Common-channel crosstalk arises from interference of optical signals of the same nominal wavelength, whereas adjacent-channel crosstalk arises from interference of optical signals of different nominal wavelengths.

Common-channel crosstalk can be distinguished into *homodyne* and *heterodyne*, depending on whether the optical frequencies of two interferers are the same or not, respectively. A special case of homodyne crosstalk arises when signals originating from the same source and following different paths arrive to the receiver (*multipath homodyne crosstalk*). Multipath homodyne crosstalk terms share the same modulation, but in general, experience different propagation delays, attenuations, phase changes, and polarization changes due to environmental fluctuations. If the optical path length difference between two multipath homodyne crosstalk signals is smaller than the coherence length of the laser, their beating is called *coherent* crosstalk, and otherwise is called *incoherent* crosstalk.

The exact crosstalk penalty in the receiver performance depends on the modulation, frequency, phase, and polarization of the interfering electric fields (see Appendix A). However the modulation, phase, and polarization of optical signals are not taken into account in the wavelength-domain representation. If a new crosstalk term is generated by a network component, it is not correct to add its power to the average power of the signal at this wavelength bin. Therefore, for simulation purposes, each interferer is represented separately as a distinct narrowband optical signal. The crosstalk induced penalty is evaluated during the second simulation step (see Section II-E).

For illustration, Fig. 2(a) shows the computer representation of an optical signal produced by a laser source contaminated by ASE noise and six multipath interferers. Without loss of generality, only five nodes of the wavelength grid are shown. All signal power is concentrated into the third wavelength bin (black

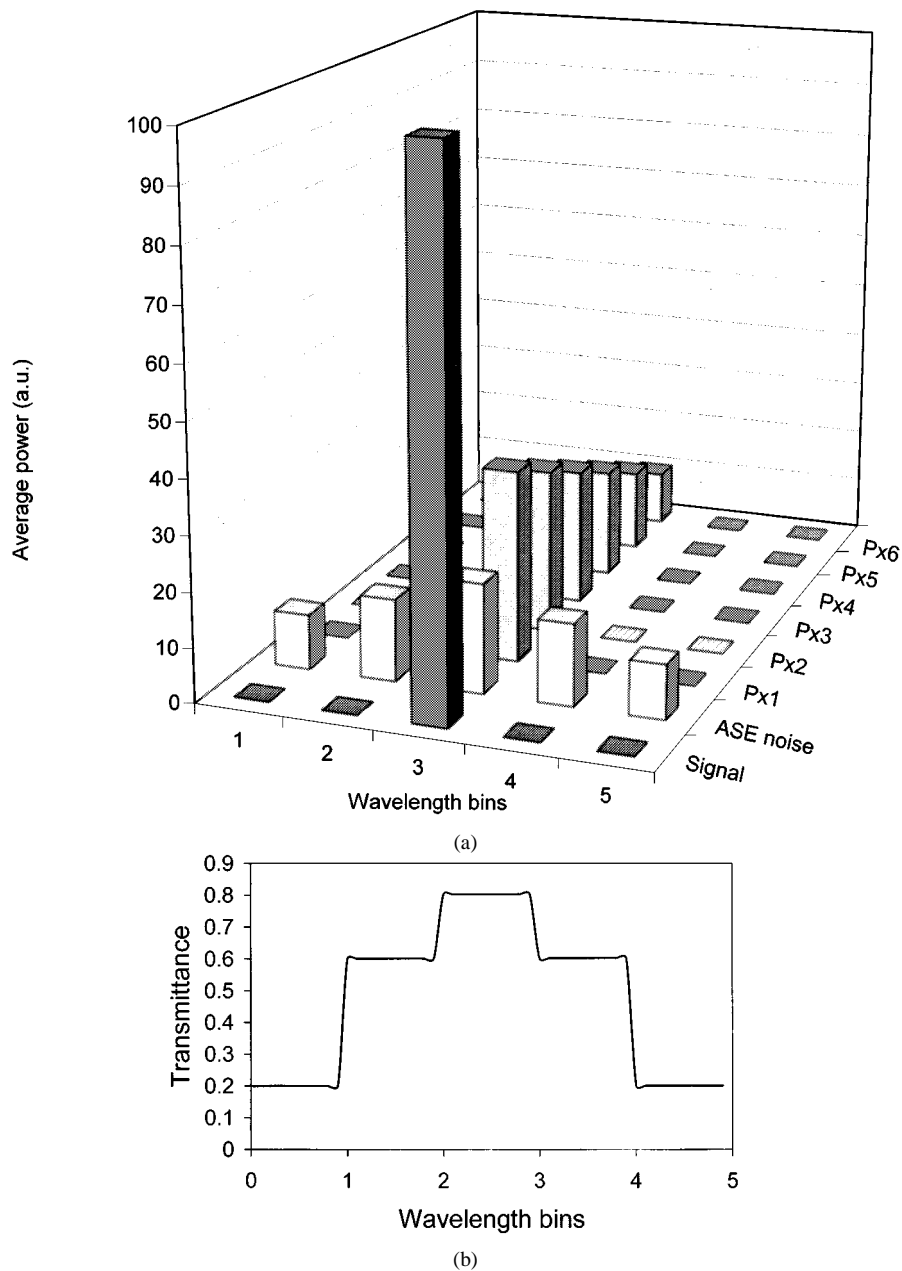


Fig. 2. (a) Wavelength-domain representation of an optical signal produced by a laser source contaminated by ASE noise and six multipath interferers. Symbols: signal: black column; ASE noise: white columns; multipath interferers, x_1-x_6 : gray columns. (b) Transmittance transfer function of an optical component.

column). ASE noise power is distributed into all five wavelength bins (white columns). The six multipath interferers, denoted by x_1-x_6 , are represented by distinct gray columns in the same wavelength bin as the optical signal.

If M different laser sources are used in the network, the complete wavelength-domain representation of the optical signals at each point in the network consists of a set of M graphs similar to Fig. 2(a).

D. Wavelength-Domain Representation of Optical Network Components

Optical network components are described in the wavelength-domain in terms of the values of their transmittance transfer functions (i.e., gain/loss) at the nodes of the wavelength grid.

These values can be given either by an analytical relationship or as a table of measured values. The gain or loss is assumed to be approximately constant within a single wavelength bin, but may be different for signals at adjacent wavelength bins. The gain or loss may also vary as a function of input power or time, but this variation is slow compared to the bit period (quasistatic components). The phase-transfer functions of the network components are discarded.

An example of transmittance transfer function of an optical component (e.g., optical filter) is shown in Fig. 2(b). Similar to Fig. 2(a), only five nodes of the wavelength grid are shown.

As optical signals, ASE noise, and optical crosstalk pass from one module to the other, their average powers at the N grid nodes are multiplied by the corresponding values of the gain/loss of the modules. It is thus possible to evaluate

the average powers of optical signal, ASE noise, and optical crosstalk at every point in the network.

Finally, performance evaluation is done using analysis or waveform-level simulation, as explained below.

E. Waveform-Level Simulation Procedure

The assumptions used in wavelength-domain simulation impose certain limitations on the phenomena that can be studied. For example, signal distortion cannot be described in the wavelength domain and must be studied analytically or numerically, using waveform-level simulation.

Consider the network topology of Fig. 3(a). During the second simulation step, only selected optical paths [e.g., the one denoted by a bold line in Fig. 3(a)] are modeled. Waveform-level representation of the optical signals and optical network components is used. The main difference between our approach and the conventional waveform-level simulation approaches is that here, instead of replicating the whole network topology, the optical path under study is reduced to an equivalent channel. The equivalent channel is constructed using the information provided by the wavelength-domain tool. The exact model of the equivalent channel may differ depending on the topology. Fig. 3(b) and (c) shows tentative models that can be used for the study of distortion due to linear and nonlinear effects, respectively.

In Fig. 3(b), the amplitude of the waveform generated at the transmitter is scaled at the received level, as calculated during the first simulation step. To study the effect of chromatic dispersion during propagation through the optical fiber and other dispersive optical components, an all-pass filter with quadratic phase can be used [34]. Signal distortion arising from filtering [35] can also be taken into account in a similar way and is not shown in Fig. 3(b). For Monte Carlo simulations, ASE noise can be modeled as a complex zero-mean additive white Gaussian noise (AWGN) with variance equal to the average ASE power calculated during the first simulation step. Dominant crosstalk terms can be simulated as separate signals. Pseudorandom generators can be used to choose their modulation, frequency, phase, and polarization. Since the information about their statistics is lost during the wavelength-domain simulation, assumptions must be made by the user. Smaller crosstalk terms are usually negligible and can be omitted. If necessary, they can be modeled in the form of noise. The statistics of this noise depend on the topology and the number of crosstalk terms.

Although the block diagram shown in Fig. 3(b) is considerably simpler than the network topology of Fig. 3(a), Monte Carlo simulation is impractical for the evaluation of low error probabilities [36] and can be used only for qualitative estimations of the performance degradation based on eye diagrams. In practice, a semianalytical technique [36] must be used in order to evaluate the performance degradation due to the combined effects of signal attenuation, ASE noise, linear optical crosstalk, and distortion.

For networks with linear and nonlinear segments, the block diagram shown in Fig. 3(c) must be used. Linear network segments [e.g., nodes 1–5 in Fig. 3(a)], which might have thou-

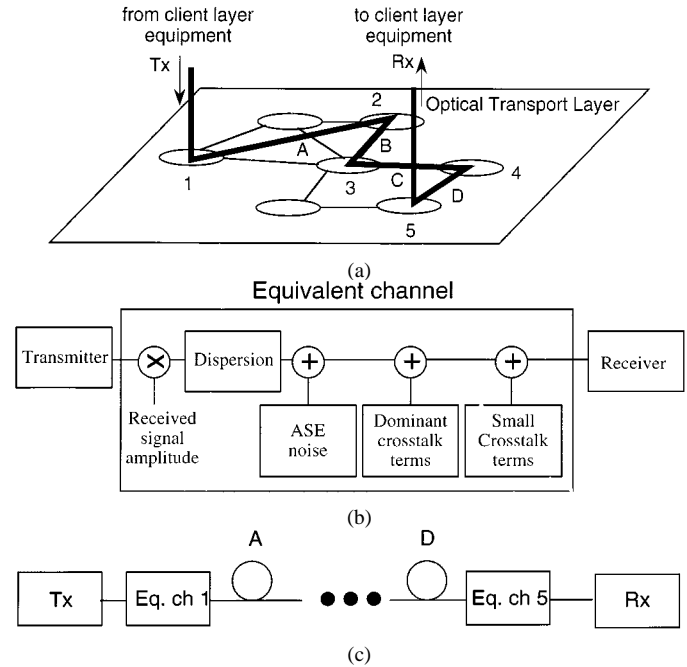


Fig. 3. (a) Example of a given network topology; (b) linear waveform-level model of the optical path denoted by a bold line in (a); (c) nonlinear waveform-level model of the optical path denoted by a bold line in (a). The details of the equivalent channels 1–5 are the same as in (b). Abbreviations: Tx = Transmitter, Rx = Receiver.

sands of optical network components, are modeled by equivalent channels. Nonlinear segments [e.g., fiber spans A–D in Fig. 3(a)] are modeled using conventional digital signal processing techniques. Assumptions about the phase of the signals must be made at the interfaces between linear and nonlinear segments since the phase information is discarded during wavelength-domain simulation.

III. FEATURES OF THE SIMULATION ENVIRONMENT

The above discussion is independent of the implementation of the network simulator. This Section focuses on the desirable features of a simulation environment used for the development of a network simulation tool with wavelength-domain and waveform-level capabilities.

The simulation program should be organized in modular form. This requirement stems from the nature of the network. Network components are represented by separate modules. Each module is implemented as a function or subroutine. It is characterized by a small number of parameters that can be easily determined from nondestructive measurements. Modules are used as building blocks of the main simulation program.

Due to the large number of modules, creation of the main simulation program using a text editor is impractical and prone to error. Therefore, the use of an input graphic user interface (GUI) is necessary. In the GUI, each module is associated with a graphical object (icon). The combination of icons allows a pictorial representation of optical systems and networks in a block diagram form. The GUI automatically translates the block diagram to main program and unambiguously schedules the order of execution of modules. The GUI allows user-friendly programming requiring little or no programming expertise.

The GUI should allow hierarchical (multilevel) modeling of the simulation modules. Each module can be built of lower level modules, and so on. This representation reflects the way a network is constructed. As the design becomes larger and more complex, this feature allows writing concise programs.

The ability to define abstract data types to represent optical signals in the wavelength domain, and to perform operations on abstract data types is essential (see Section IV-B).

A graphic output interface (GOI) is necessary for the visualization of the signals and off-line calculations.

The flow control provided by a conventional waveform-level time-domain simulation environment is sufficient for both wavelength-domain and waveform-level simulations. This is based on the following fact: waveform-level time-domain simulation is driven by a clock that advances at discrete-time intervals equal to the sampling period [9, pp. 558–560]. The main program successively calls all the routines of the modules at each instant of the simulation clock. The execution is carried out in a sample-by-sample basis, i.e., at each call, a module accepts one signal sample from each one of its input ports and produces one sample on each one of its output ports. The order of execution of modules is set using the following criterion: the outputs of a module can be computed only when the current values of all inputs are available. The procedure is organized in a loop fashion to repeat itself until the end of simulation time.

It is worth noting that the notion of time in simulation is closely related with the notion of iteration. Different instants of the simulation clock correspond to different iterations.

During wavelength-domain simulation, this iterative procedure can be used to calculate the power of the optical signal, ASE noise, and linear optical crosstalk at all points in the network. The execution is carried out in a block-by-block basis, i.e., at each call, a module accepts the whole set of parameters (i.e., power spectra of optical signals, of ASE noise, and of linear optical crosstalk) from each one of its input ports and produces a set of parameters on each one of its output ports. In network chains (i.e., open-loop network topologies) one iteration is enough to compute the steady-state optical power spectra at every point: the execution starts from the known power spectra at the beginning of the chain (i.e., laser sources) and proceeds all the way to the end, resolving the equations set with successive substitutions. In closed-loop topologies (e.g., rings, meshes, etc. . . .), several iterations are needed for convergence at the steady state. The generalization of this technique for transient power computations is straightforward [10].

IV. MONET NETWORK SIMULATION TOOL

A. Library of Optical Modules

For the MONET project, a network simulation tool was implemented based on the simulation principles presented in Section II. SPW (signal processing worksystem) [37], a communication systems-oriented commercial software product, was used as a simulation environment for the implementation.³ In addition to the desirable features presented in Section III, SPW has

an extensive library of built-in communications and signal-processing modules that can be used for waveform-level simulation. Custom-coded blocks can be written in C language, which is advantageous for creating and manipulating linear-linked lists [39].

The organization of the MONET simulation tool is shown in Fig. 4. An indicative list of modules is given on the right-hand side (RHS) of Fig. 4. The modules of the optical library are divided into three hierarchical categories, namely, Network Elements, Network Element Components, and Elementary Units. Each module is implemented using different designs, technologies, and simulation models, and can have uni- or bidirectional fiber interfaces, steady-state or dynamic properties, and so forth. Modules can be combined in any order to simulate various WDM network topologies.

For example, on the top left-hand side (LHS) of Fig. 4, two interconnected networks are shown. The Network Elements are represented by circles. At the next hierarchical level, the architecture of a simplified unidirectional WADM [11] without automatic protection switching and network control and management capabilities is shown. The depicted WADM consists of (1) two EDFA's; (2) a MUX–DMUX pair; (3) 2×2 optical switches for signal adding/dropping; and (4) variable attenuators for power equalization. The EDFA's are placed at the inputs and outputs of the WADM to compensate for the transmission losses and insertion losses of the network element components. At the next lower hierarchical level, the structure of the EDFA's is shown. In this particular example, the EDFA's are identical single-stage forward-pumped amplifiers, composed of (5) two isolators; (6) a laser diode; (7) a wavelength selective coupler (WSC); (8) a strand of erbium-doped fiber (EDF); and (9) an ASE rejection filter with notch at the noise peak at 1532 nm.

In the simulation example of Section V, wavelength terminal multiplexers (WTM's) and 4×4 WSXC's are used. Their operation is explained below.

The block diagram of a WTM is shown in Fig. 5. It consists of a laser array and a booster EDFA in one direction, a preamplifier, a demultiplexer, and a receiver array in the opposite direction. The laser array consists of eight DFB lasers and a passive combiner. The laser and receiver arrays notionally are not parts of the optical transport layer, but represent the input/output signals from/to the MONET compliant client interface [11].

The block diagram of an eight wavelength 4×4 WSXC is shown in Fig. 6. The module has four input and four output fibers (i.e., transport interfaces) carrying eight wavelengths each. The structure is similar to that of WADM's. The heart of the WSXC is eight layers of 4×4 optical-switch fabrics, one for each wavelength, which are used to reconfigure the wavelengths among the transport interfaces. In this example, the 4×4 optical-switch fabrics are composed of six 2×2 optical switches arranged in a Benes architecture (Fig. 6, inset). This particular architecture is rearrangeably nonblocking (i.e., any idle input can be connected to any idle output provided that existing connections may be rearranged) [40].

B. Implementation of the Wavelength-Domain Representation

In the MONET simulation tool, different data types are used to represent the optical signal, ASE noise, and linear optical

³An earlier wavelength-domain implementation of an EDFA using SPW was reported in [38].

MONET Optical Transport Layer Simulation

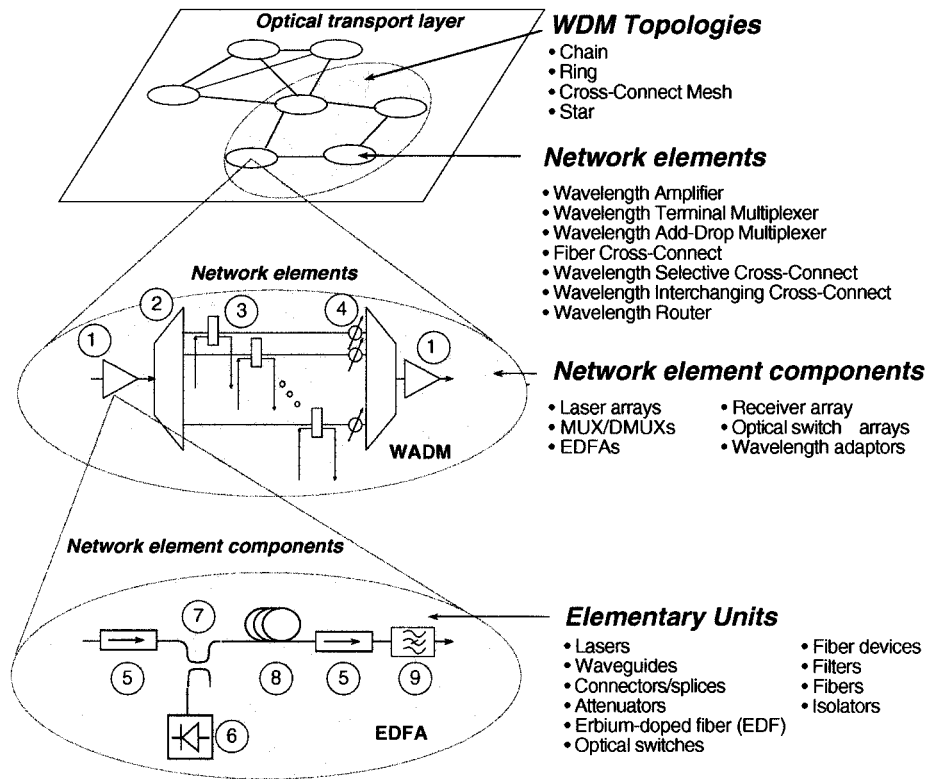


Fig. 4. Organizational chart of the MONET optical transport layer simulation tool. Left: Example of the hierarchical modeling of a network composed of wavelength add-drop multiplexers (WADM's). Successive magnifications show the different hierarchical levels. [Symbols: (1) erbium-doped fiber amplifiers (EDFA's); (2) multiplexer/demultiplexer (MUX/DMUX); (3) optical 2 × 2 switches; (4) variable attenuators for power equalization; (5) optical isolator; (6) laser diode; (7) wavelength selective coupler (WSC); (8) erbium-doped fiber (EDF); (9) ASE rejection filter]. Right: Indicative list of WDM topologies, Network Elements, Network Element Components and Elementary Units.

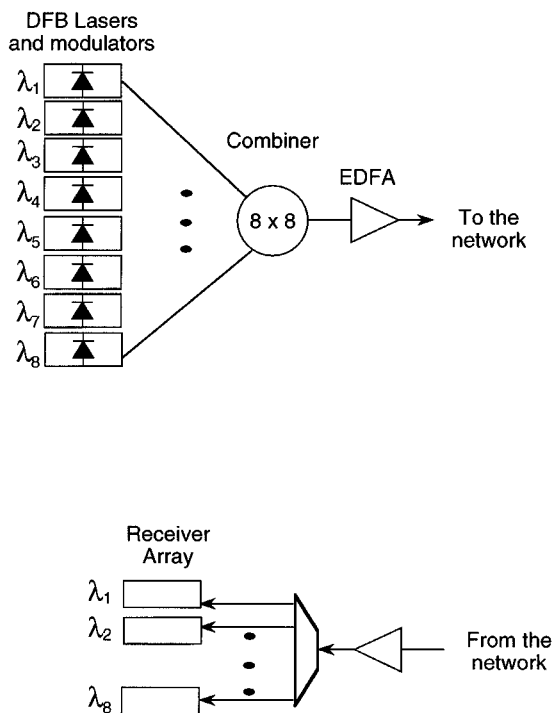


Fig. 5. Block diagram of a wavelength terminal multiplexer (WTM).

crosstalk powers in the wavelength domain. The objective is to minimize memory use and enable dynamic memory allocation for the crosstalk terms, since their exact number is unknown at the beginning of the simulation. In the following, each data type is explained separately.

In Fig. 7, the i th individual optical signal is represented by a source identification number ID_i , the signal wavelength λ_i , the signal power P_{s_i} , and a list of the most important multipath homodyne crosstalk terms $P_{x_{ij}}$, $i = 1, 2, \dots, j = 1, 2, \dots$.

- A unique identification number ID_i is assigned to each laser source. This number allows the modules to distinguish crosstalk terms originating from the same laser source and group them together.
- The wavelength λ_i of the optical signal is necessary to all modules of the wavelength-domain simulation tool that are wavelength selective.
- When optical signals pass through different modules, their powers P_{s_i} are multiplied by the transfer function coefficients of each module.
- Finally, the multipath homodyne crosstalk terms $P_{x_{ij}}$, $j = 1, 2, \dots$ of the i th individual optical signal are retained in a list. At the laser output this list is empty. At each block the list is updated with new elements. However, it is possible that the size of the crosstalk lists could become

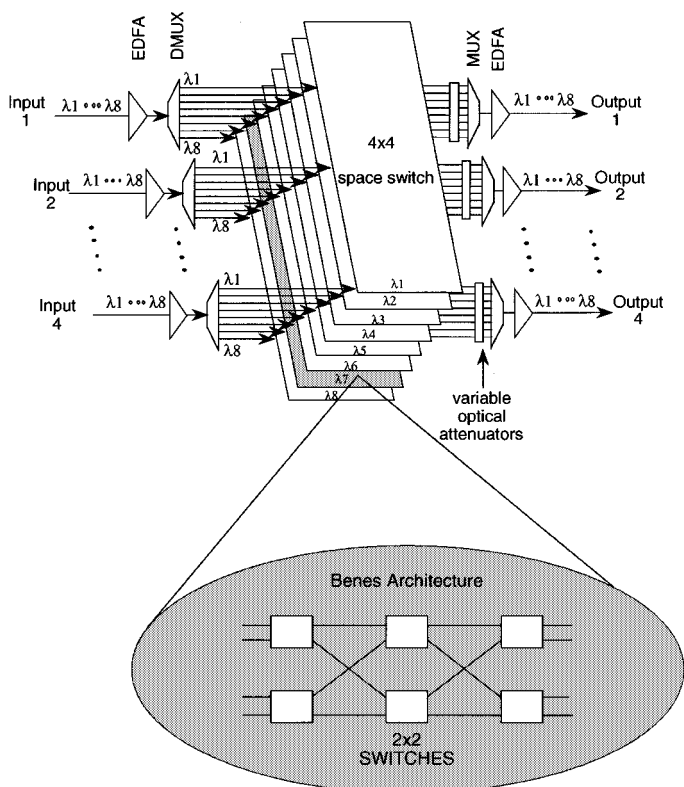


Fig. 6. Block diagram of a wavelength-selective cross-connect (WSXC).

exceedingly large. For this reason, only the most important terms are listed. A statistical description can be maintained for the discarded crosstalk terms (e.g., histogram) but it is not shown in Fig. 7.

A WDM optical signal can be represented by a list of individual optical signals. WDM signal lists can grow without limit but their final size will be small since only a limited number of laser sources will be simulated.

ASE noise is simply modeled by an array $[P_{Nk}]$ of M elements. Each element of the array represents the ASE noise power in a wavelength bin with central wavelength λ_k , $k = 1, \dots, M$. Multipath interference of ASE noise is not taken into account. In Appendix B, it is shown that whenever ASE noise arrays are added, the power of the sum of interfering noise components is equal to the sum of their powers, unless noise components are correlated. In MONET, due to the large wavelength spacing and the technology of the filters used, ASE noise correlation is small and can be safely neglected.

V. SIMULATION EXAMPLE: STUDY OF A MESH TOPOLOGY

The wavelength-domain capabilities of the MONET simulation tool were used in the past to study automatic gain control in EDFA's and EDFA chains [41], network topologies [42]–[44], and network functionalities [10], [45]. To further illustrate the operation of the wavelength-domain simulator, an additional simulation example is given below. The purpose of this example is to show that wavelength-domain simulation allows for the study of complex network topologies.

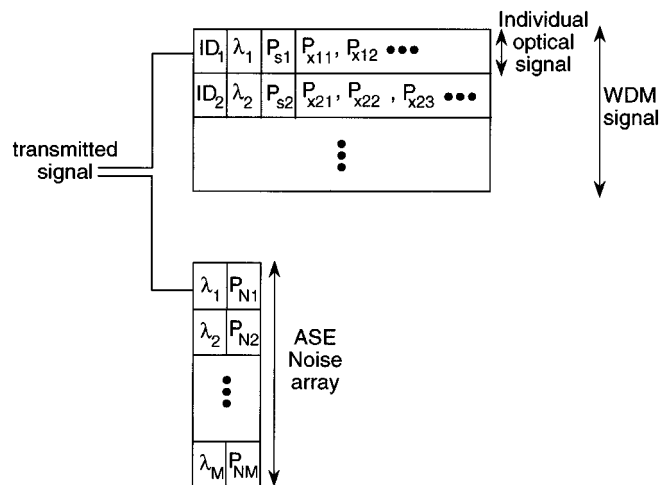


Fig. 7. Wavelength-domain representation of the optical signals, ASE noise and linear optical crosstalk in the MONET network simulation tool (Symbols: ID_i = identification number, λ_i = wavelength, P_{s_i} = signal power, $P_{x_{ij}}$ = multipath homodyne crosstalk power, P_{Nk} = ASE noise power. Subscript $i = 1, 2, \dots$ denotes the i th individual optical signal, subscript $j = 1, 2, \dots$ denotes the j th dominant multipath homodyne crosstalk term, and subscript $k = 1, 2, \dots, M$ = denotes the k th wavelength bin).

The block diagram of the network to be modeled is shown in Fig. 8. Nine network elements are connected with 11 duplex fiber links. Bidirectional WADM's, composed of two units like the one shown in Fig. 4, one for each direction, are used. Three 4×4 WSXC's are used for dynamic wavelength routing between the two WADM rings. WTM's No. 8 and No. 9 give the capability to WSXC's No. 3 and No. 4, respectively, to add-drop wavelengths. The combination of a WTM with a WSXC provides a functionality similar to the cross-connect architecture proposed by [46]. All links are assumed to have the same length. The generalization to the case of unequal fiber links is straightforward. Protection switching for link and node failure restoration is not considered in this example.

Up to eight wavelengths equally spaced at 200 GHz in the range from 1549.315 to 1560.606 nm are used for transmission between network elements [11]. More than one wavelength channel can be assigned between two network elements depending on traffic demands. Wavelength reuse is employed when possible. In our example, the eight wavelengths are used to establish five one-wavelength, nine two-wavelength, and one three-wavelength duplex connections.

A routing scenario is chosen where all eight wavelengths are present at all fibers. This routing scenario is not imposed from an inherent limitation of the wavelength-domain simulation tool, but is attractive for the following reasons. 1) Since all links are of equal length, similar operating conditions apply at the inputs of all network elements. Consequently, the EDFA's in all network elements are assumed identical. If a different number of channels are used at each path, EDFA's in each network element must be designed differently in order to give flat gain at the output. As an alternative, fixed-gain EDFA's could be used. 2) To satisfy the requirement that all fibers must carry the same number of wavelengths, routing is suboptimum and a wavelength may pass through all network elements before arriving at its destination. This results in crosstalk enhancement. In a real network,

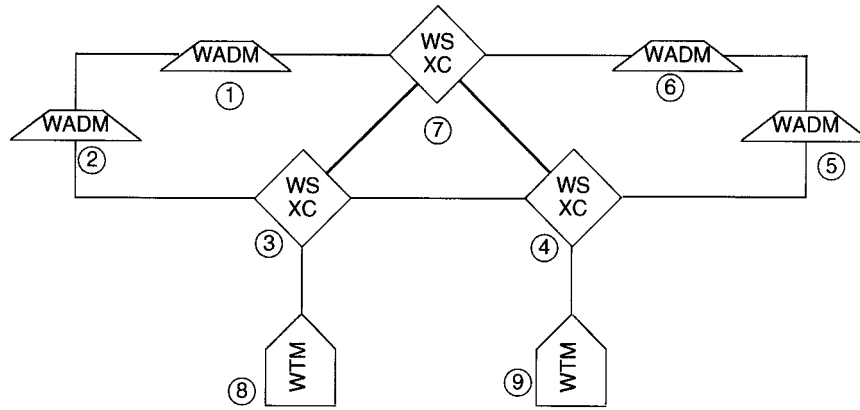


Fig. 8. Block diagram of a mesh of 4×4 wavelength-selective cross-connects (WSXC's) and wavelength add-drop multiplexers (WADM's).

wavelength allocation and routing algorithms use different criteria that would not necessarily fill all links with eight wavelengths (see, for example, [47]–[51]).

The heart of the simulation are the EDFA, MUX/DMUX, and switch modules, since they are an essential part of all network elements. The proper choice of the simulation model for the EDF is critical for the accuracy of the results and execution speed. The steady-state EDF model of [52], [53], and [10] is shown to be reasonably accurate for low-gain amplifiers (i.e., up to about 20 dB/channel) [54], [55]. Additional experimental validation of the EDF model by [52] and [53] can be found in [56]. The EDF length and pump power are adjusted to compensate for the span loss and to provide flat gain within ± 0.5 dB for all channels.

The MUX/DMUX's in the WADM's are composed of eight elementary multilayer interference (MI) filters in cascade [57]. The elementary MI filters can be approximated by third-order Butterworth filters with full-width at half maximum (FWHM) of 125 GHz [42]. In [42, Fig. 3], measurements of the transmittance of a MI eight-channel MUX were compared to simulation results based on the above approximation and were shown to be in excellent agreement.

A generalized 2×2 optical-switch module is used. A generalized switch is represented by its state, the insertion losses at the bar and cross states, and the crosstalk levels at the bar and cross states. The switching speed is neglected in this example.

All simulation parameters are listed in Table I.

The number of possible add-drop configurations depends on the number and the allowable states of the optical switches in the network elements. In the topology under study, there are 16 2×2 optical switches in each bidirectional MONET WADM (Fig. 4), eight for each direction, and eight 4×4 optical switches in each WSXC. Since a Benes architecture is used for the implementation of the 4×4 optical switches, each one of them can be set in $4! = 24$ states (i.e., equal to the number of possible permutations between the inputs of the switch). The number of possible add-drop scenarios for the mesh network of Fig. 8 is then $2^{16 \times 4} \times 24^{8 \times 3} \approx 2.5 \times 10^{52}$. Obviously, it is impossible to perform an exhaustive study of all possible add-drop configurations. Therefore, we limit our interest in a worst-case add-drop scenario.

TABLE I
WAVELENGTH-DOMAIN SIMULATION
PARAMETERS FOR THE MESH NETWORK OF FIG. 8.

<i>General simulation parameters</i>	
Simulation bandwidth (nm)	1500-1600
Resolution bandwidth (GHz)	10
Maximum number of dominant crosstalk terms/signal listed	100
Signal wavelengths (nm)	1549.315-1560.606
Channel spacing (GHz)	200
Signal power (WTM input) (dBm)	-13
Signal power (WADM input) (dBm)	1.7
Fiber loss (dB)	17
<i>EDFA</i>	
Pump power (mW)	60
Pump wavelength (nm)	980
EDF length (m)	45
Average gain/channel (dB)	17
Noise figure (1550 nm)(dB)	4.2
<i>Individual MUX/DMUX</i>	
Insertion loss (dB)	3.3
Crosstalk level (dB)	< -38
<i>Optical 2x2 switch</i>	
Insertion loss (dB)	1
Crosstalk level (dB)	-30

The worst optical path in this network passes through all network elements (e.g., three WSXC's, four WADM's, and two WTM's in the order 9-4-5-6-7-3-4-7-1-2-3-8). Transmission along this path is done using wavelength eight for which the amplifier gain is slightly under 17 dB (16.7 dB). This worst-case scenario, although improbable, provides some safety margin in the design and allows for future network growth.

Fig. 9 presents the power spectral density (PSD) at the receiver of WTM No. 8. The optical SNR is 28 dB at wavelength eight (measured in a 0.1-nm bandwidth), which is above the level required for error-free transmission at 10 Gb/s in the ab-

sence of crosstalk [58]. The total common-channel crosstalk power (not depicted in Fig. 9) is about 17 dB below the signal power and the total first adjacent-channel crosstalk power is 42 dB below the signal power.

Fig. 10 shows a histogram of the crosstalk terms at wavelength λ_s . Due to the steep transfer functions of the MI filters, multipath homodyne crosstalk from the MUX/DMUX's is small and the crosstalk introduced by the optical switches is dominant. Three first-order crosstalk terms are created at each pass from a 4×4 Benes switch fabric. Therefore, at the receiver, there are 18 first-order common-channel crosstalk terms. The received signal power is -2 dBm and the crosstalk level of the individual optical 2×2 switches is -30 dB. The group of crosstalk terms at -32 dBm corresponds to first-order crosstalk from the optical 4×4 switches, the group of crosstalk terms at -62 dBm corresponds to second order crosstalk from the optical 4×4 switches, and the group of crosstalk terms at -78 dBm corresponds to second-order crosstalk from the MUX/DMUX pairs.

In reality, due to the closed loops in the mesh, there is an infinity of higher-order crosstalk terms. In simulation, only crosstalk terms up to a finite order can be counted. Higher-order terms than the ones depicted in Fig. 10 are very small and contribute very little to the power penalty, therefore, they are neglected.

The histogram indicates that the distribution of crosstalk power is not continuous but discrete. Crosstalk terms of the same order are concentrated close together in a narrow range. In practice, small deviations of the parameters of network element components from their nominal values will tend to make this distribution continuous, smearing the peaks shown in Fig. 10.

Figs. 9 and 10 provide only a qualitative estimation of the system's performance. Despite the high value of optical SNR, the quality of the received signal might be unacceptable due to common-channel crosstalk-induced penalty. To investigate the above issue, a second simulation step using Monte Carlo simulation can be undertaken to evaluate the performance degradation due to crosstalk. This approach is used in [44]. Here, analysis is used instead.

In the analysis, different assumptions concerning the modulation, frequency, phase, and polarization of the interfering electric fields can be made. Assuming that all 18 first-order common-channel crosstalk terms are copolarized, homodyne, and interfere incoherently, it is shown [17] that the above level of common-channel crosstalk could lead to an error floor. The crosstalk level of the individual 2×2 optical switches must be reduced to -38.8 dB in order to give a crosstalk penalty that is certain to be less than 1 dB for an error probability equal to 10^{-9} . Alternatively, dilated optical switch architectures can be used [43].

The total number of simulated modules in this example is 2558. Using a resolution bandwidth of 10 GHz, the execution time is about 2 h on a Sun Sparc 5.

VI. SUMMARY

This paper presents the major principles of an efficient simulation method for the study of the optical transport layer of linear multiwavelength optical networks. The implementation of a net-

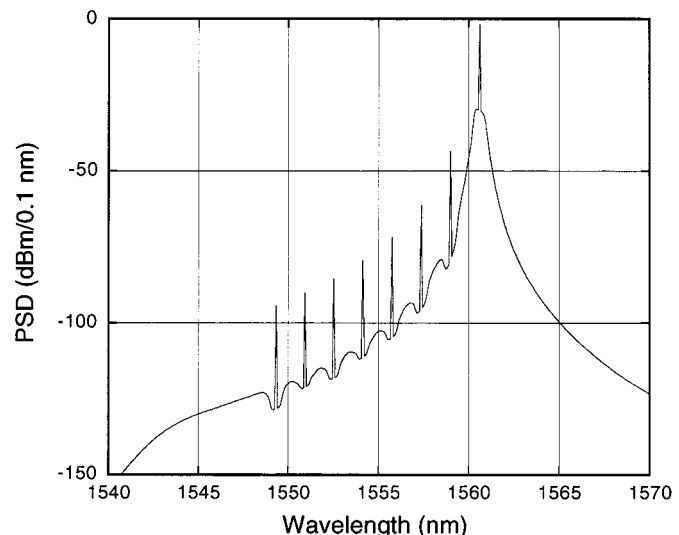


Fig. 9. Power spectral density (PSD) at the receiver used for the detection of wavelength λ_s in the wavelength terminal multiplexer (WTM) No. 8.

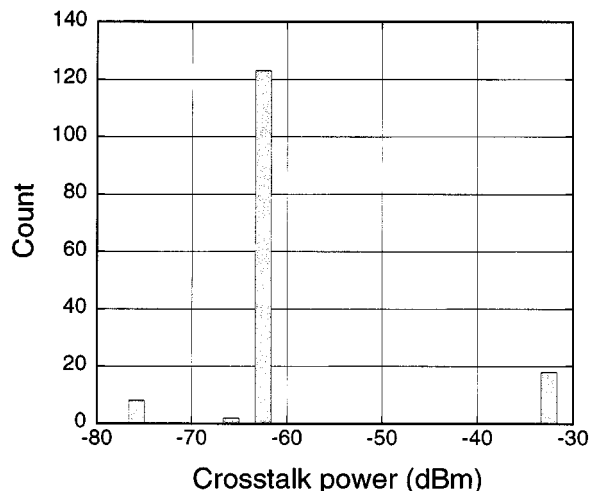


Fig. 10. Histogram of the dominant crosstalk terms at wavelength λ_s at the receiver of wavelength terminal multiplexer (WTM) No. 8.

work simulation tool based on the above method in the context of the MONET project is described. To illustrate the capabilities of the MONET simulator, a mesh of 4×4 wavelength selective cross-connects and WADM's is studied and the crosstalk performance is determined.

APPENDIX A CROSSTALK MODELING AND CLASSIFICATION

Consider a certain point in the network where there are M signals with wavelengths $\lambda_1, \dots, \lambda_M$ (not necessarily distinct) and optical powers P_1, \dots, P_M , respectively. The total electric field can be written in a phasor notation

$$\vec{E} = \sum_{j=1}^M \vec{E}_j e^{i\omega_j t} \quad (1)$$

where \vec{E}_j is the complex envelope and ω_j is the carrier angular frequency of the j th signal.

Assume that from the M received electric fields, only one (e.g., \vec{E}_k) represents the signal. The other $M - 1$ electric fields are spurious. The optical power is

$$\begin{aligned}
 P &= \frac{1}{2} |\vec{E}|^2 = \frac{1}{2} \sum_{i=1}^M \sum_{j=1}^M \vec{E}_i \vec{E}_j^* e^{i(\omega_i - \omega_j)t} \\
 &= \frac{1}{2} |\vec{E}_k|^2 + \Re \left\{ \sum_{\substack{j=1 \\ j \neq k}}^M \vec{E}_k \vec{E}_j^* e^{i(\omega_k - \omega_j)t} \right\} \\
 &\quad + \Re \left\{ \sum_{\substack{i=1 \\ i \neq k}}^M \sum_{\substack{j=1 \\ j \neq i, k}}^M \vec{E}_i \vec{E}_j^* e^{i(\omega_i - \omega_j)t} \right\} + \frac{1}{2} \sum_{\substack{i=1 \\ i \neq k}}^M |\vec{E}_i|^2 \quad (2)
 \end{aligned}$$

where \Re denotes the real part.

On the RHS of (2), the first term represents the signal power, the second term represents *signal-crosstalk* beating, the third term represents *crosstalk-crosstalk* beating and the fourth term represents *directly detected* crosstalk. Only the beatings that fall within the receiver electrical bandwidth will eventually contribute to the power.

It is observed that the significance of crosstalk terms depends on the relative polarization, frequency, phase, and modulation of the interfering electric fields. During the wavelength-domain simulation, this information is lost. Therefore, the crosstalk-induced penalty cannot be evaluated in the wavelength domain. During the first simulation step, all interferers are generated and represented by their powers, which are functions of $|\vec{E}_j|$, $j = 1, \dots, M$, respectively. During the second simulation step, (2) is evaluated based on the values of $|\vec{E}_j|$, $j = 1, \dots, M$ provided by the first simulation step, and assuming arbitrary modulations, frequencies, phases, and polarizations of the interfering electric fields.

APPENDIX B

MULTIPATH INTERFERENCE OF ASE NOISE

The interference between ASE noise components following different paths is the subject of this Appendix. It is shown that whenever ASE noise arrays are added, the power of the sum of interfering noise components is approximately equal to the sum of their powers, if the correlation between noise components is small. A closed-form expression is derived for the relative error due to the omission of the noise correlation term. It is shown that in MONET, due to the large wavelength spacing and the technology of the filters used, ASE noise correlation can be safely neglected.

Consider a WDM signal composed of N wavelength channels, which arrives at the input of a WADM. It is assumed that only two wavelength channels λ_1, λ_2 are not dropped at the WADM. Fig. 11(a) shows a simplified diagram of the WADM where an EDFA is followed by a MUX/DMUX pair with two interconnected branches for λ_1, λ_2 . The 2×2 optical switches and the servo-controlled attenuators between the MUX/DMUX are omitted. Their loss-transfer functions can be included in the transfer functions of the MUX/DMUX pair. ASE noise from the

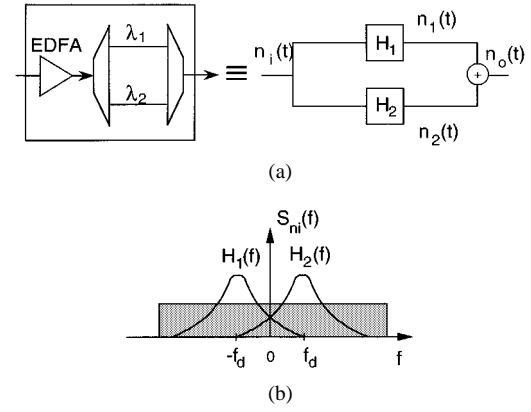


Fig. 11. (a) Cascade of an EDFA and a MUX/DMUX pair with two branches used to separate and recombine two wavelength channels λ_1, λ_2 (left) and its low-pass equivalent block diagram (right). (b) Equivalent low-pass representation of the filters $H_1(f), H_2(f)$ and input ASE noise power spectral density $S_{ni}(f)$ (shaded rectangle).

EDFA is split in the two branches of the DMUX and is recombined at the MUX output. The arrangement shown at the LHS of Fig. 11(a) is equivalent to the simplified block diagram at the RHS of Fig. 11(a) where the two branches of the MUX-DMUX pair are modeled as two elementary optical filters tuned to different central frequencies connected in parallel.

In the following, for mathematical convenience, we make use of the equivalent low-pass representation of ASE noise and elementary optical filters [14]. The input ASE noise is modeled as a complex zero-mean AWGN. Its equivalent low-pass power spectral density $S_{ni}(f)$ (shaded rectangle) and the equivalent low-pass transfer functions of the filters $H_1(f), H_2(f)$ are shown in Fig. 11(b). The equivalent low-pass transfer functions of the filters are assumed to be centered at frequencies $\pm f_d$, respectively, symmetric to the origin of axes, where $2f_d$ represents the channel spacing.

The ASE noise $n_o(t)$ at the output of the MUX can be written in equivalent low-pass notation $n_o(t) = n_1(t) + n_2(t)$, where $n_1(t), n_2(t)$ are the complex envelopes of the noises at each input of the MUX.⁴ The autocorrelation function $R_{n_o n_o}(\tau)$ of the output noise is defined as [59]

$$\begin{aligned}
 R_{n_o n_o}(\tau) &\triangleq E \{ n_o(t + \tau) n_o^*(t) \} \\
 &= R_{n_1 n_1}(\tau) + R_{n_2 n_2}(\tau) + R_{n_1 n_2}(\tau) \\
 &\quad + R_{n_2 n_1}(\tau) \quad (3)
 \end{aligned}$$

where $R_{n_1 n_1}(\tau), R_{n_2 n_2}(\tau)$ are the autocorrelation functions of the noises $n_1(t), n_2(t)$, respectively, and $R_{n_1 n_2}(\tau), R_{n_2 n_1}(\tau)$ are the cross-correlation functions between the noises $n_1(t), n_2(t)$.

The noise power $\sigma_{n_o}^2$ at the output of the MUX is then given by $R_{n_o n_o}(0)$. We can rewrite (3) in the form

$$\sigma_{n_o}^2 = \sigma_{n_1}^2 + \sigma_{n_2}^2 + \sigma_x^2 \quad (4)$$

where $\sigma_{n_1}^2, \sigma_{n_2}^2$ denote the powers of $n_1(t), n_2(t)$, respectively, and σ_x^2 denotes the power related to their cross-correlation

$$\sigma_x^2 \triangleq R_{n_1 n_2}(0) + R_{n_2 n_1}(0). \quad (5)$$

⁴Noises are treated as scalars. Their relative polarization is neglected.

Equation (4) is the formal mathematical expression of the well-known result that addition of two noises does not imply addition of their respective powers, unless noises are uncorrelated.

From (4), it is straightforward to see that the relative error ϵ_r in the evaluation of the output power $\sigma_{n_o}^2$ due to the omission of the term σ_x^2 representing the cross-correlation is given by

$$\epsilon_r \triangleq \frac{\sigma_x^2}{\sigma_{n_o}^2} \simeq \frac{\sigma_x^2}{\sigma_{n_1}^2 + \sigma_{n_2}^2}. \quad (6)$$

We are going to show that this error ϵ_r has a closed-form expression

$$\epsilon_r = \frac{2\Re \left[\int_{-\infty}^{\infty} H_1(f)H_2^*(f) df \right]}{\int_{-\infty}^{\infty} |H_1(f)|^2 df + \int_{-\infty}^{\infty} |H_2(f)|^2 df} \quad (7)$$

where \Re denotes the real part and $*$ denotes the complex conjugate.

Relationship (7) shows that the relative error ϵ_r depends exclusively on the filter characteristics. The relative error ϵ_r vanishes for orthogonal filters, i.e., filters, which satisfy the relationship

$$\int_{-\infty}^{\infty} H_1(f)H_2^*(f) df = 0. \quad (8)$$

Obviously, all filters that do not spectrally overlap are orthogonal.

A. Proof of (7)

We want to evaluate the cross-correlation function defined as

$$R_{n_1 n_2}(\tau) \triangleq E \{n_1(t+\tau)n_2^*(t)\}. \quad (9)$$

We express $n_1(t)$ and $n_2(t)$ as a convolution between the ASE noise $n_i(t)$ at the input of the DMUX and the impulse responses $h_1(t)$ and $h_2(t)$ of the filters

$$\begin{aligned} R_{n_1 n_2}(\tau) &= E \{ [h_1(t+\tau) * n_i(t+\tau)] [h_2^*(t) * n_i^*(t)] \} \\ &= E \left\{ \int_{-\infty}^{\infty} \int_{-\infty}^{\infty} h_1(t+\tau-t')h_2^*(t-t'') \right. \\ &\quad \left. \times n_i(t'+\tau)n_i^*(t'') dt' dt'' \right\} \\ &= \int_{-\infty}^{\infty} \int_{-\infty}^{\infty} h_1(t+\tau-t')h_2^*(t-t'') \\ &\quad \times E [n_i(t'+\tau)n_i^*(t'')] dt' dt'' \\ &= \int_{-\infty}^{\infty} \int_{-\infty}^{\infty} h_1(t+\tau-t')h_2^*(t-t'') \\ &\quad \times R_{n_i n_i}(t'+\tau-t'') dt' dt'' \end{aligned} \quad (10)$$

where $R_{n_i n_i}(t)$ is the autocorrelation function of the input ASE noise. Since input ASE noise is assumed to be white, its autocorrelation function is given by

$$R_{n_i n_i}(t) = \sigma_{n_i}^2 \delta(t) \quad (11)$$

where $\sigma_{n_i}^2$ is the variance of the equivalent lowpass input ASE noise and $\delta(t)$ is the Dirac delta function.

By substituting (11) into (10) we obtain

$$R_{n_1 n_2}(\tau) = \sigma_{n_i}^2 \int_{-\infty}^{\infty} h_1(t'+\tau)h_2^*(t') dt'. \quad (12)$$

In order to obtain an expression of $R_{n_1 n_2}(\tau)$ in terms of the transfer functions $H_1(f)$, $H_2(f)$ of the filters instead of the impulse responses $h_1(t)$, $h_2(t)$ we are using the Fourier transform

$$h_i(t) = \int_{-\infty}^{\infty} H_i(f)e^{i\omega t} df \quad i = 1, 2. \quad (13)$$

By substituting (13) into (12) we obtain

$$R_{n_1 n_2}(\tau) = \sigma_{n_i}^2 \int_{-\infty}^{\infty} H_1(f)H_2^*(f)e^{i\omega\tau} df. \quad (14)$$

Since $R_{n_1 n_2}(\tau) = R_{n_2 n_1}^*(\tau)$, by substituting (14) into (5), we finally obtain

$$\sigma_x^2 = 2\Re [R_{n_1 n_2}(0)] = 2\sigma_{n_i}^2 \Re \left[\int_{-\infty}^{\infty} H_1(f)H_2^*(f) df \right]. \quad (15)$$

By similar calculations, it is straightforward to see that the terms $\sigma_{n_1}^2$, $\sigma_{n_2}^2$ in (4) are given by

$$\sigma_{n_k}^2 = \sigma_{n_i}^2 \int_{-\infty}^{\infty} |H_k|^2(f) df \quad k = 1, 2. \quad (16)$$

By substituting (15) and (16) into (6), the relative error ϵ_r is given by

$$\epsilon_r = \frac{2\Re \left[\int_{-\infty}^{\infty} H_1(f)H_2^*(f) df \right]}{\int_{-\infty}^{\infty} |H_1(f)|^2 df + \int_{-\infty}^{\infty} |H_2(f)|^2 df}. \quad \square \quad (17)$$

B. Numerical Example

The purpose of this example is to investigate if we can use addition of the powers of the interfering ASE components for the modeling of ASE multipath crosstalk in the wavelength-domain representation and evaluate the relative error ϵ_r .

For simplicity, we assume that the transfer functions $H_1(f)$, $H_2(f)$ are identical and are produced by shifting the same transfer function $H(f)$, which is centered around the origin, to the positions $\pm f_d$, respectively. Then, (7) gives

$$\epsilon_r = \frac{\Re \left[\int_{-\infty}^{\infty} H(f+f_d)H^*(f-f_d) df \right]}{\int_{-\infty}^{\infty} |H(f)|^2 df}. \quad (18)$$

Using the triangular inequality, (18) gives an upper bound of the relative error

$$|\epsilon_r| \leq \frac{\int_{-\infty}^{\infty} |H(f + f_d)| |H(f - f_d)| df}{\int_{-\infty}^{\infty} |H(f)|^2 df}. \quad (19)$$

It is assumed that the squared magnitude of the transfer functions of MUX–DMUX's used in MONET can be approximated by a third-order Butterworth filter [42]. Since a MUX–DMUX pair is equivalent to a cascade of two such filters, $|H(f)|$ is given by

$$|H(f)| = \frac{1}{1 + \left(\frac{f}{f_{3\text{db}}}\right)^6}. \quad (20)$$

By substituting (20) into (19), we finally obtain

$$|\epsilon_r| \leq \frac{\int_{-\infty}^{\infty} \left[1 + \left(\frac{f + f_d}{f_{3\text{db}}}\right)^6\right]^{-1} \left[1 + \left(\frac{f - f_d}{f_{3\text{db}}}\right)^6\right]^{-1} df}{\int_{-\infty}^{\infty} \left[1 + \left(\frac{f}{f_{3\text{db}}}\right)^6\right]^{-2} df}. \quad (21)$$

For typical values $f_{3\text{db}} = 50$ GHz and $f_d = 100$ GHz, numerical integration of (21) gives $|\epsilon_r| \leq 0.12\%$. In practice, the relative error is slightly larger if we consider multipath interference of ASE noise from all MUX–DMUX branches. In any case, the relative error is very small and can be neglected.

ACKNOWLEDGMENT

The authors are grateful to Dr. J. L. Zyskind, Dr. R. E. Tench, Dr. E. L. Goldstein, Dr. F. Shehadeh, Dr. J. Y. Pan, Dr. R. S. Vodhanel, and Dr. V. Shah for their help during this work, and to L. M. Szemiot for corrections in the syntax of the manuscript.

REFERENCES

- [1] Virtual Photonics, Photonic Transmission Design Suite. [Online]. Available: <http://www.virtualphotonics.com/>
- [2] A. F. Elrefaie, "Computer-aided modeling and simulation of lightwave systems," *IEEE LEOS Newslett.*, vol. 7, p. 1, Feb. 19–20, 1993.
- [3] ARTIS. OptSim. [Online]. Available: <http://www.artis.it>
- [4] C. Glingener, J. P. Elbers, and E. Voges, "Simulation tool for WDM networks," in *Colloquium on WDM Technol. Applicat.*. London, U.K.: Inst. Elect. Eng., 1997, vol. 1, pp. 2/1–2/4.
- [5] ZEDO. FOCUS. [Online]. Available: <http://focuss.zedo.fuedo.de>
- [6] C. Le Brun, E. Guillard, and J. Citerne, "Communication systems interactive software (COMSIS): modeling of components and its application to the simulation of optical communication systems," *Appl. Opt.*, vol. 37, pp. 6059–6065, Sept. 1998.
- [7] RSoft. LinkSIM. [Online]. Available: <http://www.rsoftinc.com>
- [8] K. S. Shanmugan, "Simulation and implementation tools for signal processing and communication systems," *IEEE Commun. Mag.*, pp. 36–40, July 1994.
- [9] M. C. Jeruchim, P. Balaban, and K. S. Shanmugan, *Simulation of Communication Systems*. New York: Plenum, 1992.
- [10] I. Roudas, D. H. Richards, N. Antoniadis, J. L. Jackel, and R. E. Wagner, "An efficient simulation model of the Erbium-doped fiber for the study of multiwavelength optical networks," *Opt. Fiber Technol.*, vol. 5, pp. 363–389, Oct. 1999.
- [11] R. E. Wagner, R. C. Alferness, A. A. M. Saleh, and M. S. Goodman, "MONET: Multiwavelength optical networking," *J. Lightwave Technol.*, vol. 14, pp. 1349–1355, June 1996.
- [12] I. Roudas, N. Antoniadis, D. H. Richards, J. L. Jackel, and R. E. Wagner, "Wavelength-domain simulation: An efficient technique for the design of multiwavelength optical networks," in *Integr. Photon. Res. Top. Meet.*. Santa Barbara, CA, July 1999.
- [13] M. A. Marsan, S. Benedetto, E. Biglieri, V. Castellani, M. Elia, L. Lo Presti, and M. Pent, "Digital simulation of communication systems with TOPSIM III," *IEEE J. Select. Areas Commun.*, vol. SAC-2, pp. 29–42, Jan. 1984.
- [14] J. G. Proakis and D. G. Manolakis, *Digital Signal Processing: Principles, Algorithms and Applications*, 3rd ed. Englewood Cliffs, NJ: Prentice-Hall, 1996.
- [15] G. P. Agrawal, *Nonlinear Fiber Optics*. New York: Academic, 1995.
- [16] S. Rotolo, S. Brunazzi, R. Cadeddu, E. Casaccia, and C. Cavazzoni, "Strategy for a computer-aided analysis of all-optical multiwavelength transparent networks," in *Opt. Fiber Commun. Conf. (OFC)*, 1995, pp. 205–206.
- [17] E. L. Goldstein, L. Eskildsen, and A. F. Elrefaie, "Performance implications of component crosstalk in transparent lightwave networks," *IEEE Photon. Technol. Lett.*, vol. 6, pp. 657–660, May 1994.
- [18] E. L. Goldstein, L. Eskildsen, C. Lin, and Y. Silberberg, "Polarization statistics of crosstalk-induced noise in transparent lightwave networks," *IEEE Photon. Technol. Lett.*, vol. 7, pp. 1345–1347, Nov. 1995.
- [19] D. J. Blumenthal, P. Granstrand, and L. Thylen, "BER floors due to heterodyne coherent crosstalk in space photonic switches for WDM networks," *IEEE Photon. Technol. Lett.*, vol. 8, pp. 284–286, Feb. 1996.
- [20] J. Zhou, M. J. O'Mahony, and S. D. Walker, "Analysis of optical crosstalk effects in multi-wavelength switched networks," *IEEE Photon. Technol. Lett.*, vol. 6, pp. 302–305, Feb. 1994.
- [21] J. Zhou, R. Cadeddu, E. Casaccia, C. Cavazzoni, and M. J. O'Mahony, "Crosstalk in multiwavelength optical cross-connect networks," *J. Lightwave Technol.*, vol. 14, pp. 1423–1435, June 1996.
- [22] E. Iannone and R. Sabella, "Analysis of wavelength-switched high-density WDM networks employing wavelength conversion by four-wave-mixing in semiconductor optical amplifiers," *J. Lightwave Technol.*, vol. 13, pp. 1579–1592, July 1995.
- [23] R. Sabella and E. Iannone, "Optical transport networks employing all-optical wavelength conversion: limits and features," *J. Lightwave Technol.*, vol. 14, pp. 968–978, June 1996.
- [24] Y. D. Jin and M. Kavehrad, "An optical cross-connect system as a high-speed switching core and its performance analysis," *J. Lightwave Technol.*, vol. 14, pp. 1183–1197, June 1996.
- [25] H. Takahashi, K. Oda, and H. Toba, "Impact of crosstalk in an arrayed-waveguide multiplexer on $N \times N$ optical interconnection," *J. Lightwave Technol.*, vol. 14, pp. 1097–1105, June 1996.
- [26] C.-S. Li and F. Tong, "Crosstalk and interference penalty in all-optical networks using static wavelength routers," *J. Lightwave Technol.*, vol. 14, pp. 1120–1126, June 1996.
- [27] P. J. Legg, M. Tur, and I. Andonovic, "Solution paths to limit interferometric noise induced performance degradation in ASK/direct detection lightwave networks," *J. Lightwave Technol.*, vol. 14, pp. 1943–1954, Sept. 1996.
- [28] M. Gustavsson, L. Gillner, and C. P. Larsen, "Statistical analysis of interferometric crosstalk: Theory and optical network examples," *J. Lightwave Technol.*, vol. 15, pp. 2006–2019, Sept. 1997.
- [29] S. L. Danielsen, C. Joergensen, B. Mikkelsen, and K. E. Stubkjaer, "Analysis of interferometric crosstalk in optical switch blocks using moment generating functions," *IEEE Photon. Technol. Lett.*, vol. 10, pp. 1635–1637, Nov. 1998.
- [30] K. P. Ho, "Analysis of co-channel crosstalk interference in optical networks," *Electron. Lett.*, vol. 34, pp. 383–385, Feb. 1998.
- [31] K.-P. Ho, "Analysis of homodyne crosstalk in optical networks using Gram-Charlier series," *J. Lightwave Technol.*, vol. 17, pp. 149–153, Feb. 1999.
- [32] G. P. Agrawal, *Fiber-Optic Communication Systems*. New York: Wiley, 1992.
- [33] K. Feher, *Advanced Digital Communications Systems and Signal Processing Techniques*. Englewood Cliffs, NJ: Prentice-Hall, 1987, ch. 9, pp. 459–487.
- [34] A. F. Elrefaie, R. E. Wagner, D. Atlas, and D. G. Daut, "Chromatic dispersion limitations in coherent lightwave transmission systems," *J. Lightwave Technol.*, vol. 6, pp. 704–709, May 1988.

- [35] I. Roudas, N. Antoniadis, R. E. Wagner, and L. D. Garrett, "Influence of realistic optical filter characteristics on the performance of multiwavelength optical networks," in *IEEE/LEOS Ann. Meet.*, vol. 2, Nov. 1997, pp. 542–543.
- [36] M. C. Jeruchim, "Techniques for estimating the bit error rate in the simulation of digital communication systems," *IEEE J. Select. Areas Commun.*, vol. SAC-2, pp. 153–170, Jan. 1984.
- [37] Alta group, *Signal Processing Worksystem, Version 3.5*: Cadence Design Systems, Inc., Feb. 1996.
- [38] S. L. Zhang and J. J. O'Reilly, "EDFA custom-coded simulation block for use in WDM optical fiber communication system studies," *Simulation*, vol. 63, pp. 377–385, Dec. 1994.
- [39] B. W. Kernighan and D. M. Ritchie, *The C Programming Language*. Englewood Cliffs, NJ: Prentice-Hall, 1978.
- [40] H. S. Hinton, *An Introduction to Photonic Switching Fabrics*. New York: Plenum, 1993.
- [41] D. H. Richards, J. L. Jackel, and M. A. Ali, "A theoretical investigation of dynamic all-optical automatic gain control in multichannel EDFA's and EDFA cascades," *IEEE J. Select. Topics Quantum Electron.*, vol. 3, pp. 1027–1036, Aug. 1997.
- [42] N. Antoniadis, I. Roudas, R. E. Wagner, and S. F. Habiby, "Simulation of ASE noise accumulation in a wavelength add-drop multiplexer cascade," *IEEE Photon. Technol. Lett.*, vol. 9, pp. 1274–1276, Sept. 1997.
- [43] N. Antoniadis, I. Roudas, R. E. Wagner, J. L. Jackel, and T. E. Stern, "Crossstalk performance of a wavelength selective cross-connect mesh topology," in *Opt. Fiber Commun. Conf. (OFC)*, San Jose, CA, Feb. 1998, Paper FJ4.
- [44] N. Antoniadis, I. Roudas, R. E. Wagner, T. E. Stern, J. L. Jackel, and D. H. Richards, "Use of wavelength- and time-domain simulation to study performance degradations due to linear optical crosstalk in WDM networks," *OSA TOPS, Opt. Net. Appl.*, vol. 20, pp. 288–293, 1998.
- [45] D. H. Richards, J. L. Jackel, I. Roudas, W. Xin, N. Antoniadis, and M. A. Ali, "Method for detecting fiber cuts in a WDM ring with saturated EDFAs," in *Opt. Fiber Commun. Conf. (OFC)*. San Diego, CA, Feb. 1999, FJ4.
- [46] G. R. Hill, P. J. Chidgey, F. Kaufhold, T. Lynch, O. Sahlen, M. Gustavsson, M. Janson, B. Lagerstrom, G. Grasso, F. Meli, S. Johansson, J. Ingers, L. Fernandez, S. Rotolo, A. Antonielli, S. Tebaldini, E. Vezzoni, R. Caddedu, N. Caponio, F. Testa, A. Scavennec, M. J. O'Mahony, J. Zhou, A. Yu, W. Sohler, U. Rust, and H. Herrmann, "A transport network layer based on optical network elements," *J. Lightwave Technol.*, vol. 11, pp. 667–679, May/June 1993.
- [47] I. Chlamtac, A. Ganz, and G. Karmi, "Lightpath communications: An approach to high bandwidth optical WAN's," *IEEE Trans. Commun.*, vol. 40, pp. 1171–1182, July 1992.
- [48] K. C. Lee and V. O. K. Li, "A wavelength convertible optical network," *J. Lightwave Technol.*, vol. 11, pp. 962–970, May/June 1993.
- [49] R. A. Barry and P. A. Humblet, "On the number of wavelengths and switches in all-optical networks," *IEEE Trans. Commun.*, vol. 42, pp. 583–591, Feb./Mar./Apr. 1994.
- [50] K. Bala, T. E. Stern, D. Simchi-Levi, and K. Bala, "Routing in a linear lightwave network," *IEEE/ACM Trans. Networking*, vol. 3, pp. 459–469, Aug. 1995.
- [51] R. Ramaswami and K. N. Sivarajan, "Routing and wavelength assignment in all-optical networks," *IEEE/ACM Trans. Networking*, vol. 3, pp. 489–500, Oct. 1995.
- [52] A. A. M. Saleh, R. M. Jopson, J. D. Evankow, and J. Aspell, "Modeling of gain in Erbium-doped fiber amplifiers," *IEEE Photon. Technol. Lett.*, vol. 2, pp. 714–717, Oct. 1990.
- [53] R. M. Jopson and A. A. M. Saleh, "Modeling of gain and noise in Erbium-doped fiber amplifiers," in *Fiber Laser Sources and Amplifiers III*: SPIE, 1991, vol. 1851, pp. 114–119.
- [54] E. Desurvire, *Erbium-Doped Fiber Amplifiers: Principles and Applications*. New York: Wiley, 1994.
- [55] C. R. Giles and E. Desurvire, "Modeling Erbium-doped fiber amplifiers," *J. Lightwave Technol.*, vol. 9, pp. 271–283, Feb. 1991.
- [56] S. Ovadia and C. Lin, "Performance characteristics and applications of hybrid multichannel AM-VSB/M-QAM video lightwave transmission systems," *J. Lightwave Technol.*, vol. 16, pp. 1171–1186, July 1998.
- [57] M. A. Scobey and D. E. Spock, "Passive DWDM components using microplasma optical interference filters," in *Opt. Fiber Conf.: Tech. Dig.*, San Jose, CA, Feb. 1996, pp. 242–243.
- [58] P. A. Humblet and M. Azizoglu, "On the bit error rate of lightwave systems with optical amplifiers," *J. Lightwave Technol.*, vol. 9, pp. 1576–1582, Nov. 1991.
- [59] A. Papoulis, *Probability, Random Variables and Stochastic Processes*, 3rd ed. New York: McGraw-Hill, 1991.

Ioannis Roudas was born in 1966 in Athens, Greece. He received the diploma of physics and the Certificate of electronics and radio-engineering from the University of Athens, Greece, in 1988 and 1990, respectively, and the M.S. and Ph.D. degrees from ENST Paris, France, in 1991 and 1995, respectively. His Ph.D. thesis concerned modeling and optimal design of coherent optical communication systems.

During 1995–1998, he was with the Optical Networking Research Department at Bell Communications Research, Red Bank, NJ, where he was involved in the Multiwavelength Optical Networking (MONET) project. His research mainly focused on the development of an efficient computer representation of the MONET optical transport layer. In parallel, during the fall semesters 1997 and 1998, he taught the graduate course "Lightwave Systems" as an Adjunct Professor of Electrical Engineering at Columbia University.

Since 1999, he has been a Senior Research Scientist in the Photonic Research and Test Center of Corning Inc., Somerset, NJ. His current research concerns modeling of transmission effects in high data rate optical communications systems and networks.

Dr. Roudas serves as a Reviewer for the IEEE/OSA JOURNAL OF LIGHTWAVE TECHNOLOGY and the IEEE PHOTONICS TECHNOLOGY LETTERS.

Neophytos Antoniadis (S'93–M'98) received the B.S., M.S., M.Phil., and Ph.D. degrees all in electrical engineering from Columbia University, New York, NY, in 1992, 1993, 1996, and 1998, respectively.

His Ph.D. work at Columbia University focused on modeling of optical components, WDM communication systems and networks. During the period of 1994 to 1998, he participated in research work at Bellcore, Red Bank, NJ, and was involved in both the Optical Networks Technology Consortium (ONTC) as well as the Multi-wavelength Optical Networking (MONET) programs. Within MONET, Dr. Antoniadis was a part of a team that designed and developed a wavelength-domain computer simulator for studying performance impairments in WDM optical networks.

In 1998, he joined Corning Inc. at the Photonic Research & Test Center, Somerset, NJ, where he is currently a Senior Research Scientist doing research on advanced fiber optic systems and networks to support development of telecommunication fiber and optical network elements.

Dr. Antoniadis is a Member of the IEEE and currently holds one patent with two others pending in the field of fiber optics.

Dwight H. Richards (S'95–M'98) was born in St. Mary, Jamaica, in 1967. He received the B.E. and the M.E. degrees, both in electrical engineering from the City College of New York in 1993 and 1996, respectively. He then completed the Ph.D. degree at the Graduate School of the City University of New York in 1999. His current research interests include optical communication networks with an emphasis on simulation methodologies. Dr. Richards has been with Telcordia Technologies (formerly Bellcore) since 1996, where he is currently a member of technical staff.

Richard E. Wagner is Manager of Optical Network Research at Corning Incorporated, having joined that effort in early 1998. Prior to that, he was a Director at Bellcore, where he was the Bellcore Project Manager of the Multiwavelength Optical Networking (MONET) program since its start in December 1994. The MONET program involved research into national-scale configurable WDM networks. From 1986 until 1994, he was responsible for managing research in heterodyne lightwave systems technology at Bellcore. Before 1986, he was with Bell Laboratories, where he supervised an undersea transmission group that investigated 1300 nm and 1550 nm singlemode lightwave systems. From 1976 to 1980, he was involved with exploratory development of multimode lightwave connectors, switches, and multiplexers.

Dr. Wagner has been the Chair of the Photonics Division of the Optical Society of America, and Chair of the Optical Networks Technical Group of LEOS. He was associated with organizing the OFC conference for more than 15 years, and has helped to organize more than 20 other international conferences in fiber optics. He has authored or coauthored more than one-hundred-fifty papers and holds four patents in the field of fiber optics.

Dr. Wagner received the B.S. and M.S. degrees in mechanical engineering from the Ohio State University in 1969, and the Ph.D. degree in optics from the Optical Sciences Center at the University of Arizona in 1976.

Janet Lehr Jackel (M'93–SM'97) was born in Queens, New York in 1947. She received the B.A. degree in physics from Brandeis University, Waltham, MA in 1969, and the M.S. and Ph.D. degrees, both in physics, from Cornell University in 1972 and 1976. From 1976–1983, she worked at Bell Laboratories in the field of integrated optics. In 1984, with the breakup of AT&T, she joined the newly-formed Bellcore, where she has continued to work on a variety of research topics ranging from materials to devices to systems, but all connected with optical communications. Her current research focuses on the interaction of optical components in multiwavelength optical network.

Dr. Jackel is a Fellow of the Optical Society of America and a Senior Member of the IEEE.

Sarry F. Habiby holds a Ph.D. in electrical engineering from Ohio State University. He is currently a Senior Manager at Tellium, Inc. and is responsible for the engineering of applications and networks as well as developing proposals and system design for Tellium customers. Prior to joining Tellium, he was with Telcordia Technologies (formerly Bellcore) for over 10 years as a key contributor to the development of optical interconnect and optical networking technologies. He was a task leader for setting system level requirements in the MONET project.

Thomas E. Stern (S'54–M'57–SM'67–F'72–LF'95) received his education at the Massachusetts Institute of Technology, obtaining the B.S. and M.S. degrees in 1953 and the Sc.D. degree in 1956, all in electrical engineering. He served in the U.S. Air Force Research and Development Command from 1956–1958, and joined Columbia University in 1958. At present, he holds the title of Dicker Professor Emeritus at Columbia.

Prof. Stern served in various leadership capacities at Columbia including Chairman of the Department of Electrical Engineering, Technical Director of the Center for Telecommunications Research (CTR), and Leader of the CTR's Lightwave Networks Research Group. He holds several patents in communications and has authored two textbooks and more than a hundred papers in networks and related fields.

Aly F. Elrefaie, photograph and biography not available at the time of publication.